Carrington, A., Pezzini, S., van Delft, MR., Schoop, L., Lotsch, B., Katsnelson, MI., ... Wiedmann, S. (2017). Unconventional mass enhancement around the Dirac nodal loop in ZrSiS. *Nature Physics*, *14*, 178-183. https://doi.org/10.1038/nphys4306

Unconventional mass enhancement around the Dirac nodal loop in ZrSiS

S. Pezzini[a), 1,2], M. R. van Delft[a),1,2], L. Schoop[3], B. Lotsch[3], A. Carrington[4], M. I. Katsnelson[2], N. E. Hussey*[1,2] and S. Wiedmann*[1,2]

[1]*High Field Magnet Laboratory (HFML-EMFL), Radboud University, Toernooiveld 7, Nijmegen 6525 ED, Netherlands.*

[2]*Radboud University, Institute for Molecules and Materials, Nijmegen 6525 AJ, Netherlands.*

[3]*Max Planck Institute for Solid State Research, Heisenbergstr. 1, 70569 Stuttgart, Germany.*

[4]*H. H. Wills Physics Laboratory, University of Bristol, Tyndall Avenue, Bristol BS8 1TL, UK.*

The topological properties of fermions arise from their low-energy Dirac-like band dispersion and associated chiralities. Initially confined to points, extensions of the Dirac dispersion to lines and even loops have now been uncovered and semimetals hosting such features have been identified. However, experimental evidence for the enhanced correlation effects predicted to occur in these topological semimetals has been lacking. Here, we report a quantum oscillation study of the nodal loop semimetal ZrSiS in high magnetic fields that reveals significant enhancement in the effective mass of the quasiparticles residing near the nodal loop. Above a threshold field, magnetic breakdown occurs across gaps in the loop structure with orbits that enclose different windings around its vertices, each winding accompanied by an additional π Berry phase. The amplitudes of these breakdown orbits exhibit an anomalous temperature dependence. These findings demonstrate the emergence of novel, correlation-driven physics in ZrSiS associated with the Dirac-like quasiparticles.

[a)] These authors contributed equally to this manuscript.

Condensed-matter systems with an energy-momentum dispersion *topologically* distinct with respect to (i.e. not adiabatically deformable into) the one of standard metals, semiconductors or insulators, represent a new exciting frontier in physics [1-5]. These materials host, in their bulk and/or surfaces, low-energy excitations mimicking relativistic particles, which opens new possibilities for the simulation of long-sought phenomena of high-energy physics, as well as for the realization of novel (quantum) information schemes. Graphene, topological insulators (TIs) and, more recently, Dirac and Weyl semimetals (WSMs) have been pioneering platforms for this research area [6,7].

The advent of nodal-line semi-metals (NLSMs) [8-12], i.e. systems in which the conduction and valence bands cross each other along a closed trajectory (line or loop) inside the Brillouin zone, has opened up a new arena for the exploration of topological aspects of condensed matter that may be distinct from those associated with TIs or WSMs [13,14]. It is claimed, for example, that due to the vanishing density of states near the Fermi level ε_F, screening of the Coulomb interaction may become weaker in NLSMs than in conventional metals and remain long-ranged [15]. This, coupled with their metallic nature, could make NLSMs more susceptible to various types of order (e.g. superconductivity, magnetism or charge order), both in the bulk [16] and on the surface [17].

While the degeneracy points in WSMs are robust against *any* perturbation that preserves translational symmetry, nodal lines or nodal loops require additional crystalline symmetries, such as mirror or non-symmorphic symmetry, to protect the extended line-like touching between the conduction and valence bands [7,14]. To date, only a few candidate NLSMs have been identified experimentally. In non-centrosymmetric $PbTaSe_2$, strong spin-orbit coupling leads to the creation of nodal rings which have been confirmed by angle-resolved photoemission spectroscopy (ARPES) [10] while in $PtSn_4$, ARPES has revealed a Dirac nodal arc structure that has been attributed to surface states [9]. In both systems, however, the topological elements of the electronic structure coexist with several other bands that cross the Fermi level ε_F.

The third experimental class to have been identified thus far is ZrSiX (X = S, Se, Te). The first of these, ZrSiS, has a number of distinct features. Firstly, it contains a diamond-shaped Fermi surface (FS) close to a line of Dirac nodes that in contrast to $PbTaSe_2$ and $PtSn_4$, is the *only* band feature near ε_F. Thus, the physical behavior of ZrSiS, be it bulk- or surface-derived, is

governed essentially by the electronic states in close proximity to the nodes. Secondly, the linear dispersion of these bands extends, in some regions of the Brillouin zone, over an energy range (2 eV) that is much larger than is found in other Dirac-like compounds. The range in which all bands are linearly dispersing is ~ 0.5 eV. Spin-orbit coupling introduces a small gap (~ 0.02 eV) in the Dirac spectrum (as illustrated by the energy contour plot shown in Fig. S1 of the Supplementary Information).

ARPES studies have confirmed the existence of the diamond-shaped FS in ZrSiS, within the (k_x, k_y) plane, in addition to a Dirac-like dispersion that extends over an energy range exceeding 1 eV [11,12]. Previous quantum oscillation studies have also reported evidence for pockets associated with the Dirac nodal loop in ZrSiS [18-21], ZrSiSe and ZrSiTe [22,23]. In each case, the topological character of these loops was inferred from the observation of a phase shift in the quantum oscillations associated with the Berry phase of the orbit.

While the topological nature of NLSMs appears to be established, evidence for enhanced many-body effects, e.g. as a precursor to any new broken symmetry phases, has yet to emerge. Here, we report a magnetoresistance study of high-quality ZrSiS single crystals up to 33 Tesla. By extending the field range of earlier studies, we are able to resolve many new Shubnikov-de Haas (SdH) oscillation frequencies at all temperatures below 60 K, including some very high frequency oscillations that arise due to magnetic breakdown across gaps along the nodal loop. The effective masses associated with these new frequencies are found to be significantly enhanced over conventional band-structure estimates. Moreover, the oscillation amplitude for the breakdown orbits exhibits an anomalous temperature dependence reminiscent of that recently found in the candidate topological Kondo insulator SmB_6 [24]. Collectively, these results provide hints that ZrSiS lies close to a quantum phase transition, possibly to some form of density wave order, and is thus an ideal material platform on which to explore novel correlation effects in topological matter.

Dirac nodal loop

The crystal structure of ZrSiS (tetragonal space group *P4/nmm*) is displayed in Fig. 1a. ZrSiS has the PbFCl-type structure (like LiFeAs) [25,26] with layers of Zr and S that are sandwiched between Si square nets extending in the *ab*-plane. The electronic band structure of bulk ZrSiS is shown in Fig. 1b. The most dominant and noteworthy feature of the electronic structure is the series of linearly-dispersing bands that cross very close to ε_F, giving rise to a nodal loop

whose location is indicated in the corresponding Fermi surface plot shown in Fig. 1c. The final assembly of loops gives rise to a diamond-shaped Fermi surface within the (k_x, k_y) plane that is quasi-two-dimensional yet strongly dispersive along k_z. Significantly, as indicated in Fig. 1b, the more parabolic bands (mostly originating from the sulphur states) are located far from the Fermi level, with the result that the Fermi surface depicted in Fig. 1c is composed uniquely from the almost-linearly dispersing bands.

Oscillatory magnetoresistance

Figure 2a shows a series of magnetoresistance (MR) sweeps up to 33 T carried out on a ZrSiS single crystal at regular temperature intervals between 1.5 K and 60 K with the magnetic field applied perpendicular to the *ab*-plane. Very similar results obtained on a second crystal are presented in Fig. S4 of the Supplementary Information. As reported previously [18,19,21,27], the MR is extremely large, reaching values of order 10^4 % in 33 T for **B**//*c*, and 7×10^5 % with the field oriented at a polar angle θ = 45°. Superimposed on top of the MR background are multiple SdH oscillations, some of which are very fast, as emphasized in the blow-up of the highest field data plotted in the right panel of Fig. 2a (the data at 1.5 K are presented in Fig. S5 over an extended field range, with and without background subtraction).

A fast Fourier transform (FFT) of the lowest temperature sweep in Fig. 2a is shown in Fig. 2b. The oscillations can be readily split into two groups; a low frequency (F < 1 kT) and a high frequency (F > 7.5 kT) group. The low frequency spectrum is dominated by two peaks. The one at 240 $\pm$ 5 T has been observed by a number of different groups [19-21] and corresponds to the α hole pocket (the 'petal') that is located at the vertex of the diamond. The second peak with a frequency of 600 $\pm$ 10 T is consistent (albeit 20% higher) than band structure estimates for the elongated β electron pocket (the 'dog-bone') that runs parallel to the top rung of the nodal loop (see Fig. 1c). A similar frequency was reported in a recent magneto-thermoelectric study [28].

The higher frequency spectrum comprises a series of peaks ranging from 7.5 kT to around 11 kT. These peaks do not correspond to any closed contour of the Fermi surface of ZrSiS shown in Fig. 1c but rather they originate from magnetic breakdown orbits that encircle the diamond. This is confirmed by a number of observations. Firstly, as indicated by the dashed lines in the right panel of Fig. 2c, the lower set of five peaks are separated by units of approximately 240 T, i.e. by the frequency of the petal orbit. The magnitude of the peaks corresponds to a series

of breakdown orbits (labelled $A \pm n\alpha$, where n is an integer) that follow the inner surface of the dog-bones with each successive peak in the FFT spectrum incorporating one additional petal. A similar assignment can be made for the second set of peaks (labelled $B \pm n\alpha$) that trace the outer surface of the dog-bones. Fig. 2e illustrates some of the possible breakdown combinations, while a full assignment is shown in Fig. S6 and Table S1 of the Supplementary Information. Taking into account the expanded β pocket, all the frequencies of the peaks in the FFT correspond to possible breakdown trajectories within the same plane, including some frequencies that would be 'forbidden' within a semi-classical picture [29].

The second telling observation is the rapid suppression of the high frequency oscillations by a small tilt of the magnetic field away from the *c*-axis. Fig. 2c contains a set of MR sweeps obtained at different polar angles θ, while Fig. 2d shows the corresponding high frequency part of the FFT spectrum for increasing θ. The oscillations (and the amplitude of the corresponding peaks) are found to be completely suppressed once $\theta > \theta_c$, with $2.2^o < \theta_c < 3.5^o$. This sudden collapse of the fast oscillations with small tilt angle is another clear indication of magnetic breakdown. As illustrated in Fig. 2f, some of the breakdown gaps must increase in size as the field is tilted. Since the tunneling probability drops exponentially with gap magnitude (or equivalently, the distance in *k*-space between adjacent elements of the breakdown orbit), the oscillation amplitude is then rapidly suppressed. A calculation of the attenuation in oscillation amplitude, plotted as a dashed line in Fig. 2g, confirms this (details of the calculation itself can be found in the Supplementary Information).

Importantly, at the magnetic fields considered, no breakdown orbits can take place in the central (Γ-X-M) plane of the Brillouin zone, due to the large gaps between the pockets (more than one order of magnitude larger than the ones separating the petal and the dog-bone in the top plane, see Fig. S2). The experimental observation of magnetic breakdown, together with its peculiar spectral features discussed above, allow therefore for a conclusive identification of the α and β pockets along the topmost portion of the nodal line.

Geometrical phase in the breakdown orbits

Having established that the different elements of the Fermi surface are tied to the nodal loop, we now turn to examine its topological character. According to the band structure calculations, the petal is located at the apex of the diamond and thus encircles a Dirac cone (see Fig. S1 of the Supplementary Information for a visualization of this). As a consequence, electrons

performing any closed circuit including a petal should acquire a π Berry phase [19]. Given that the breakdown orbits of the type A + $n\alpha$ and B + $n\alpha$ are closed trajectories that differ by an integer number of petals (see Fig. 2e), one expects there to be a relative phase shift of π between orbits with *n* even or odd. This phase shift should then be visible in the quantum oscillation trace. Figure 3 shows one such trace (black line, after subtraction of a slowly-varying background), together with two different simulations for the oscillating component of the resistance (colored lines). These simulated curves consist of a sum of cosine terms, with amplitudes and frequencies determined from the magnetic breakdown part of the FFT spectrum (the sum is limited to those components which are most clearly resolved, see Fig. 2b). The top panel simulation includes a π phase for the breakdown orbits corresponding to closed loops around an odd number of petals (*A*+α, *A*+3α, …), while the bottom panel simulation has no phase factor. The comparison between Figures 3a and 3b shows that the Berry phase must be taken into account in order to correctly describe the data, thus confirming the topological nature of ZrSiS (the data and simulation of Fig. 3a are also shown over an extended magnetic field range in Fig. S7). Moreover, magnetic breakdown orbits that selectively enclose band touching points (i.e. singularities of the Berry curvature) are shown here, for the first time, to provide a novel probe of topological systems.

These collective results, together with the more detailed angular dependent study of the low frequency oscillations illustrated in Fig. S8 of the Supplementary Information, firmly establish the topological nodal loop structure in ZrSiS that was predicted in earlier band structure calculations [12,26]. Indeed, for **B**//*c*, only minor corrections to the dog-bone orbit were required to get a consistent match with *all* of the peaks identified in the FFT. This is the first main finding of our study. In the following, we turn our attention to the quasiparticle masses extracted from these measurements and arguably the most surprising finding, namely the anomalous temperature and field dependences of the SdH oscillation amplitude.

Mass enhancement along the nodal line

Figure 4a shows a series of raw FFT spectra for both the low (left panel) and high (right panel) frequency ranges obtained from the full field sweeps performed at different temperatures between 1.5 and 60 K. By restricting the field range however, the temperature evolution of the oscillation amplitudes was found to vary, implying that the effective masses of the quasiparticles performing each orbit were actually field-dependent. The masses obtained from such spectra are shown in Fig. 4b for the petal and dog-bone orbits (see Fig. S9 of the

Supplementary Information for the corresponding temperature plots). For the petal orbit, m^* varies only slightly with field with an average value $m^* = 0.21 \pm 0.03\ m_e$, in reasonable agreement with previous low-field measurements [18,19,21] and band structure estimates of $m^* = 0.16 \pm 0.02\ m_e$.

For the dog-bone orbit, however, the situation is strikingly different. Firstly, m^* is found to have a value larger than 1.0 m_e for all field ranges. This is significantly enhanced with respect to the band-derived value of 0.55 m_e. (A 20% increase in the area of the β pocket changes the band mass by only 5 %.) Secondly, m^* is found to become heavier with increasing field strength. At the highest field range, the measured effective mass of the dog-bone orbit is almost three times heavier than the estimated band mass. Such an enhancement is beyond that expected from a conventional electron-phonon interaction and implies significant polaronic or correlation effects. Indeed, this is the largest mass enhancement ever observed for a Dirac system and is particularly striking given the extremely wide (2 eV) band width of the linear dispersion.

Discussion

According to Roy and Huh *et al*. [15,16], the specific properties of the band dispersions near ε_F in a NLSM, in particular the presence of the nodal line running parallel to the Fermi surface, imply that the Coulomb interaction is only partially screened due to a vanishing density of states (DOS). In graphene, with isolated Dirac points, electron-electron interactions are also only partially screened. This leads to a modification of the Dirac dispersion in such a way that m^* is found to shrink as ε_F approaches the Dirac point [30,31]. In ZrSiS, the Fermi line node is not actually pinned to the Fermi level and therefore the DOS does not vanish precisely at ε_F. Nevertheless, the fact that the largest mass enhancement is found for quasiparticles on the dog-bone pocket running parallel to the nodal loop suggests that residual Coulomb interactions lead to an *enhancement* in m^* rather than a reduction. Smaller, but still finite, effects are also expected for the petal orbit. Significantly, ARPES sees no renormalization of the band dispersion [11,12], suggesting that the renormalization only occurs very close to ε_F and is thus unobservable by ARPES.

This field-induced enhancement of m^* for the β pocket is reminiscent of what is observed in certain correlated electron systems such as $YbRh_2Si_2$ [32] or $CeCoIn_5$ [33] that can be tuned to a quantum critical point (QCP) by a magnetic field; the approach to the QCP is reflected in a

divergence of m^* due to a dressing of the quasiparticles by the quantum fluctuations associated with the adjacent ordered state. In NLSMs, theoretical predictions for continuous quantum phase transitions into various ordered states have emerged, both in the bulk [16] and on the surface [17], provided onsite or nearest-neighbor interactions are sufficiently strong. In ZrSiS, the additional mass enhancement in field could arise feasibly from the raising (through Zeeman splitting) of one of the spin sub-systems towards the Fermi level, which in turn (due to the vanishing DOS) leads to enhanced correlation effects. In this regard, it would certainly be interesting to explore the evolution of this enhancement to even higher fields in due course.

The final, novel finding from our study is the departure from the canonical Lifshitz-Kosevich (LK) form of the *T*-dependence of the oscillation amplitudes specifically for the breakdown orbits, representative plots of which are shown in Figure 4c. While either the low-*T* or high-*T* data can be fitted approximately using the standard LK form [34], there is a clear discontinuity in all cases at a temperature $T_0 \sim 8$ K. The corresponding effective mass extracted from the LK fit above T_0 is comparable to that obtained for the α pocket, while below T_0, it increases by approximately one order of magnitude. While the peaks associated with the *B*-group (i.e. those tracing the outer surface of the β pocket) appear to merge into a single broad peak around T_0, making their identification difficult, the *A*-group peaks remain discernible across the entire temperature range yet the *T*-dependence of their amplitudes is qualitatively the same. Moreover, in Fig. S10, we show that this behavior remains robust whichever criterion we use to analyse the temperature dependence of the FFT spectrum. We are not aware of any physical origin for such a transition, particularly given that there is no concomitant change in the Fermi surface topology (i.e in the oscillation frequencies) with temperature. Phenomenologically, this type of behavior can be attributed to a boson mode with an energy of the order of T_0 that strongly renormalizes the electron effective mass only within a non-adiabatic layer $|\varepsilon - \varepsilon_F| < T_0$, similar to the case of electron-phonon interaction [35].

The oscillation amplitude for each breakdown orbit depends not only on the effective mass associated with the orbit, but also on the probability to tunnel across the breakdown gap. Thus with increasing temperature, the magnetic breakdown may become thermally-assisted, leading to an enhancement in the tunneling probability and an upward deviation from the LK form for the oscillation amplitude. Within such a scenario, however, one might expect the deviation to be gradual [36] and not sharp as observed in ZrSiS, unless of course, the

breakdown gap itself also shrinks as the temperature is increased. It is also worth noting here that no deviations from the LK formula have been reported in other breakdown systems such as organic salts or elements such as Zn.

A recent theoretical study of quantum oscillatory phenomena in *gapped* NLSMs predicts an anomalous *T*-dependence in the oscillation amplitude [37], though not of the form reported here for ZrSiS. There, the amplitude is expected to show a non-monotonic dependence, collapsing to zero as $T \Rightarrow 0$ due to the presence of the hybridization gap. In ZrSiS, of course, the small hybridization gap is bridged at high fields by the breakdown orbits and thus the non-monotonic behavior will be absent. Nevertheless, the sharp upturn in the oscillation amplitude found in ZrSiS does not appear to be consistent with such a picture.

The sharpness of the deviation is somewhat reminiscent of the behavior reported recently [24] in the candidate topological Kondo insulator SmB_6 [38]. Despite having a bulk insulating state, quantum oscillations (in the magnetic torque) were observed below 25 K with multiple frequencies up to 15 kT [24]. Below 1 K, however a dramatic upward enhancement of the oscillation amplitude, by almost one order of magnitude, was seen in one of the low frequency orbits (F = 330 T). Knolle and Cooper have theoretically predicted QO with marked non-LK behaviour in band-inverted insulators like SmB_6 [39], but also in InAs/GaSb [40]. Although their conclusions stand in qualitative agreement with our data, certain aspects of the theory do not apply to ZrSiS. Firstly, ZrSiS is strictly semimetallic due to the energy dispersion of the nodal loop (Figure S1), and secondly the anomalous QO should not appear in the magnetotransport, as reported here, but only in the thermodynamical observables (e.g. magnetisation)[40].

Inspection of the nodal-loop Fermi surface projection of ZrSiS, shown in the inset of Fig. 4, suggests that the unusual mass enhancement on the breakdown orbits is possibly linked to enhanced, large-Q density wave correlations (spin or charge) across near-nested sections of the diamond-shaped Fermi surface. In this case, one can expect a logarithmically divergent effective mass at the threshold of instability that in principle, can make the renormalization extremely strong [41]. The effective energy scale of the relevant large-Q boson would have to be very low, however, in order to account for the marked change in the effective mass of the quasiparticles involved in the breakdown orbits around T_0. The field-enhanced mass found for the β pocket, by contrast, could arise from small-Q density-wave correlations, presumably

across the opposite faces of the dog-bone. Such a scenario requires both short- [16] and long-range [15] many-body interactions to be strongly enhanced in ZrSiS.

The field of topological semi-metals is only just emerging. The addition of correlation effects, as suggested by this present study, opens up new frontiers for the exploration of novel exotic states in these systems. Indeed, theorists have already predicted the creation of novel correlation-induced phase transitions to ordered states, both in the bulk and on the surface. Moreover, the associated quantum phase transition is believed to realize entirely new critical universality classes [17]. The work presented in this letter suggest that strong correlation effects are indeed present in ZrSiS and thus, with careful manipulation of this system, e.g. through doping studies, such novel transitions associated with the topological nodal loop, at or close to half-filling, may be induced.

Methods

Sample synthesis and characterization. Single crystals were grown out of the elements using iodine vapour transport. Stoichiometric amounts of the elements and a small amount of iodine were placed in a carbon coated quartz tube and heated to 1100°C with a 100°C temperature gradient for 1 week. The obtained crystals were subsequently annealed at 600°C for a period of 4 weeks. The crystal structure was confirmed with single-crystal x-ray and electron diffraction. All crystals were also examined by electron microscopy and back-scattered electron detectors to look for evidence of inclusions, and none were found.

Magnetotransport measurements: We studied two samples with parallel-piped shape. Six electrical contacts were defined on each sample with silver conductive paste; two of them, uniformly covering the two smaller faces of the samples, were employed as current source and drain, while the other four acted as voltage probes on different lateral sides (equivalent data were collected on the two lateral sides of the samples, indicating high homogeneity in terms of charge distribution and current flow). The resistance data were acquired in four probe configuration, with a constant current excitation of 3 mA, and standard lock-in acquisition at 13 Hz frequency. The two samples were attached to a rotating stage and simultaneously characterized in a ^{4}He VTI system with base temperature of 1.5 K. The cryogenic system was accommodated in the room-*T* access bore (32 mm diameter) of a resistive Bitter magnet at HFML, with maximum field 33 T. The samples displayed highly symmetric resistance signals with respect to the magnetic field direction, hence only data obtained for positive magnetic field orientation are shown here. The anti-symmetric signal in our magnetoresistance curves was too small to allow us to resolve any Hall component. This is consistent with reports in the literature where, e.g ρ_{xx} ~ 60 $\mu\Omega$cm and ρ_{xy} ~ 0.2 $\mu\Omega$cm at B = 9 T and T = 20 K [21].

Electronic structure calculations: Electronic structure calculations were performed using a full-potential linearized augmented plane-wave plus local orbital method as implemented in the Wien2K package [42]. The experimental lattice parameters and internal positions were used (a =3.544 Å, c = 8.055 Å, Z_{Zr} = 0.2725, Z_S= 0.6220 [25]) along with the PBE-GGA exchange correlation potential [43]. The spin-orbit interaction was included using a second variational method [42]. The calculation was converged with 10^4 k-points in the full Brillouin zone. For rendering of the Fermi surface (Fig. 1c) the energy eigenvalues were evaluated on a much more dense grid of 4 ×10^6 k -points in order to minimise interpolation errors which become severe as the Fermi level approaches the nodal line. In order to calculate accurately the

breakdown gap, an even more dense mesh with k-point spacing smaller than 10^{-3} a was necessary.

References

[1] G. E. Volovik, The universe in a helium droplet (Clarendon Press, Oxford, 2003); *Lect. Notes Phys*. **718**, 31 (2007).

[2] C. L. Kane and E. J. Mele, Z_2 topological order and the quantum spin Hall effect. *Phys. Rev. Lett.* **95**, 146802 (2005).

[3] B. A. Bernevig, T. L. Hughes, and S.-C. Zhang, Quantum spin Hall effect and topological phase transition in HgTe quantum wells. *Science* **314**, 1757 (2006).

[4] J. E. Moore and L. Balents, Topological invariants of time-reversal-invariant band structures. *Phys. Rev. B* **75**, 121306 (2007).

[5] M. Konig, S. Wiedmann, C. Brune, A. Roth, H. Buhmann, L. Molenkamp, X.-L. Qi, and S.-C. Zhang, Quantum spin Hall insulator state in HgTe quantum wells. *Science* **318**, 766 (2007).

[6] S. M. Young, S. Zaheer, J. C. Y. Teo, C. L. Kane, E. J. Mele and A. M. Rappe, Dirac semimetal in three dimensions. *Phys. Rev. Lett.* **108**, 140405 (2012).

[7] S. M. Young and C. L. Kane, Dirac semimetals in two dimensions. *Phys. Rev. Lett*. **115**, 126803 (2015).

[8] H. Weng *et al*., Topological node-line semimetal in three-dimensional graphene networks. *Phys. Rev. B* **92**, 045108, (2015).

[9] Y. Wu, L-L. Wang, E. Mun, D.D. Johnson,D. Mou, L. Huang, Y. Lee, S.L. Bud'ko, P.C. Canfield and A. Kaminski. Dirac node arcs in $PtSn_4$. *Nature Phys*. **12**, 667 (2016).

[10] G. Bian, T.-R. Chang, R. Sankar, S.-Y. Xu, H. Zheng, T. Neupert, C.-K. Chiu, S.-M. Huang, G. Chang, I. Belopolski, D. S. Sanchez, M. Neupane, N. Alidoust, C. Liu, B. Wang, C.-C. Lee, H.-T. Jeng, C. Zhang, Z. Yuan, S. Jia, A. Bansil, F. Chou, H. Lin and M. Zahid Hasan, Topological nodal-line fermions in spin-orbit metal $PbTaSe_2$, *Nature Commun.* **7**, 10556 (2016).

[11] M. Neupane, I. Belopolski, M. M. Hosen, D. S. Sanchez, R. Sankar, M. Szlawska, S-Y. Xu, K. Dimitri, N. Dhakal, P. Maldonado, P. M. Oppeneer, D. Kaczorowski, F. Chou, M. Z. Hasan and T. Durakiewicz, Observation of topological nodal fermion semimetal phase in ZrSiS, *Physical Review B* **93**, 201104(R) (2016).

[12] L. M. Schoop, M. N. Ali, C. Straβer, A. Topp, A. Varykhalov, D. Marchenko, V. Duppel, S. S.P. Parkin, B. V. Lotsch and C. R. Ast, Dirac cone protected by non-symmorphic symmetry and three-dimensional Dirac line node in ZrSiS, *Nature Commun.* **7**, 11696 (2016).

[13] A. A. Burkov, *Topological semimetals*. *Nature Mater.* **15**, 1145 (2016).

[14] C. Fang, H. Weng, Xi Dai and Z. Fang, Topological nodal line semimetals. *arXiV:1609.05414v1*

[15] Y. Huh, E.-G. Moon and Y.-B. Kim, Long-range Coulomb interaction in nodal-ring semimetals. *Phys. Rev. B* **93**, 035138 (2016).

[16] B. Roy, Interacting line-node semimetal and spontaneous symmetry breaking. *arXiV:1607.07867v1*.

[17] J. Liu and L. Balents, Correlation and transport phenomena in topological nodal-loop semi-metals, *arXiV:1609.05529v1*

[18] X. Wang, X. Pan, M. Gao, J. Yu, J. Jiang, J. Zhang, H. Zuo, M. Zhang, Z. Wei, W. Niu, Z. Xia, X. Wan, Y. Chen, F. Song, Y. Xu, B. Wang, G. Wang and R. Zhang, *Adv. Electron. Mater.* **2**, 1600228 (2016).

[19] M. N. Ali, L. Schoop, C. Garg, J. M. Lippmann, E. Lara, B. Lotsch and S. Parkin, Butterfly magnetoresistance, quasi-2D Dirac Fermi surfaces and a topological phase transition in ZrSiS. *Sci. Adv.* **2**,

[20] J. Hu, Z. Tang, J. Liu, X. Liu, Y. Zhu, D. Graf, K. Myhro, S. Tran, C.-N. Lau, J. Wei and Z. Mao, Evidence of topological nodal-line fermions in ZrSiSe and ZrSiTe. *Phys. Rev. Lett*. **117**, 016602 (2016).

[21] R. Singha, A. Pariari, B. Satpati and P. Mandal, Large non-saturating magnetoresistance and signature of non-degenerate Dirac nodes in ZrSiS, *Proc. Nat. Acad. Sci.* **114**, 2468 (2017).

[22] J. Hu, Z. Tang, J. Liu, Y. Zhu, J. Wei and Z. Mao, Evidence of Dirac cones with 3D character probed by dHvA oscillations in nodal-line semimetal ZrSiS. *arXiV:1604.01567*.

[23] A. Topp, J. Lippmann, A. Varykhalov, V. Duppel, B. V. Lotsch, C. R. Ast and L. M. Schoop, Non-symmorphic band degeneracy at the Fermi level in ZrSiTe. *New J. Phys.* (in press, 2016).

[24] B. S. Tan, Y.-T. Hsu, B. Zeng, M. Ciomaga Hatnean, N. Harrison, Z. Zhu, M. Hartstein, M. Kiourlappou, A. Srivastava, M. D. Johannes, T. P. Murphy, J.-H. Park, L. Balicas, G. G. Lonzarich, G. Balakrishnan and S. E. Sebastian, Unconventional Fermi surface in an insulating state, *Science* **349**, 287 (2015).

[25] A. Klein Haneveld and F. Jellinek, Zirconium silicide and germanide chalcogenides preparation and crystal structures. *Rec. Trav. Chim. Pays-Bas* **83**, 776 (1964).

[26] Q. Xu, Z. Song, S. Nie, H. Weng, Z. Fang and X. Dai, Two-dimensional oxide topological insulator with iron-pnictide superconductor LiFeAs structure. *Phys. Rev. B* **92**, 205310 (2015).

[27] Y.-Y. Lv, B.-B. Zhang, X. Li, S.-H. Yao, Y. B. Chen, J. Zhou, S.-T. Zhang, M.-H. Lu and Y.-F. Chen, Extremely large and significantly anisotropic magnetoresistance in ZrSiS single crystals, *Appl. Phys. Lett*. **108**, 244101 (2016).

[28] M. Matusiak, J. R. Cooper, D. Kaczorowski, Thermoelectric quantum oscillations in ZrSiS. *arXiv:1701.02137*.

[29] V. M. Gvozdikov, Yu. V. Pershin, E. Steep, A. G. M. Jansen and P. Wyder, de Haas–van Alphen oscillations in the quasi-two-dimensional organic conductor κ–$(ET)_2Cu(NCS)_2$: The magnetic breakdown approach, *Phys. Rev. B* **65**, 165102 (2002).

[30] D. C. Elias, R. V. Gorbachev, A. S. Mayorov, S. V. Morozov, A. A. Zhukov, P. Blake, L. A. Ponomarenko, I. V. Grigorieva, K. S. Novoselov, F. Guine and A. K. Geim, Dirac cones reshaped by interaction effects in suspended graphene, *Nature Phys.* **7**, 701 (2011).

[31] G. L. Yu, R. Jalil, B. Belle, A. S. Mayorov, P. Blake, F. Schedin, S. V. Morozov, L. A. Ponomarenko, F. Chiappini, S. Wiedmann, U. Zeitler, M. I. Katsnelson, A. K. Geim, K. S. Novoselov and D. C. Elias, Interaction phenomena in graphene seen through quantum capacitance. *Proc. Natl. Acad. Sci.* **110**, 3282 (2013).

[32] P. Gegenwart, J. Custers, C. Geibel, K. Neumaier, T. Tayama, K. Tenya, O. Trovarelli and F. Steglich, Magnetic-field induced quantum critical point in $YbRh_2Si_2$. *Phys. Rev. Lett.* **89**, 056402 (2002).

[33] J. Paglione, M. A. Tanatar, D. G. Hawthorn, E. Boaknin, R. W. Hill, F. Ronning, M. Sutherland, L. Taillefer, C. Petrovic and P. C. Canfield, Field-induced quantum critical point in $CeCoIn_5$. *Phys. Rev. Lett.* **91**, 246405 (2003).

[34] D. Shoenberg, *Magnetic Oscillations in Metals* (Cambridge: Cambridge University Press, 1984).

[35] J. R. Schrieffer, *Theory of Superconductivity* (Perseus Books, 1983).

[36] K. Kishigi, M. Nakano, K .Machida and Y. Hori, dHvA effect with quantum interference oscillation due to magnetic breakdown. *J. Phys. Soc. Japan* **64**, 3043 (1995).

[37] H. K. Pal, F. Piechon, J.-N. Fuchs, M. Goerbig and G. Montambaux, Quantum Oscillations in Gapped Systems. *arXiV:1604.01688v2*.

[38] M. Dzero, K. Sun, V. Galitski, and P. Coleman, Topological Kondo insulators. *Phys. Rev. Lett.* **104**, 106408 (2010).

[39] J. Knolle and N. R. Cooper, *Phys. Rev. Lett.* **115**, 146401 (2015).

[40] J. Knolle and N. R. Cooper, *Phys. Rev. Lett.* **118**, 176801 (2017).

[41] A. Virosztek and J. Ruvalds, Nested Fermi-liquid theory, *Phys. Rev. B* **42**, 4064 (1990).

[42] P. Blaha, K. Schwarz, G. K. H. Madsen, D. Kvasnicka and J. Luitz, WIEN2k, An augmented plane wave + local orbitals program for calculating crystal properties (Karlheinz Schwarz, Techn. Universität Wien, Austria, 2001). ISBN 3-9501031-1-2.

[43] J. P. Perdew, S. Burke and M. Ernzerhof, Generalized gradient approximation made simple. *Phys. Rev. Lett*. **77**, 3865 (1996).

Acknowledgements: We acknowledge enlightening discussions with Y.-B. Kim and A. McCollam. We also acknowledge the support of the HFML-RU/FOM, member of the European Magnetic Field Laboratory (EMFL). A portion of this work was supported by the Engineering and Physical Sciences Research Council (grant no. EP/K016709/1).

Author contributions: S.W. initiated the project in collaboration with L.S.. S.P., M.v.D. and S.W. performed the magnetotransport measurements. L.S. and B.L. synthesized the ZrSiS single crystals. A.C. performed the electronic band structure calculations. S.P., M.v.D., S.W., A.C., M.I.K. and N.E.H. analysed the data. N.E.H. wrote the manuscript with input from all the co-authors.

Competing financial interests: The authors declare no competing financial interests.

Materials and correspondence: Correspondence and requests for materials should be addressed to S.W. (s.wiedmann@science.ru.nl) and N.E.H. (n.e.hussey@science.ru.nl).

Figure 1

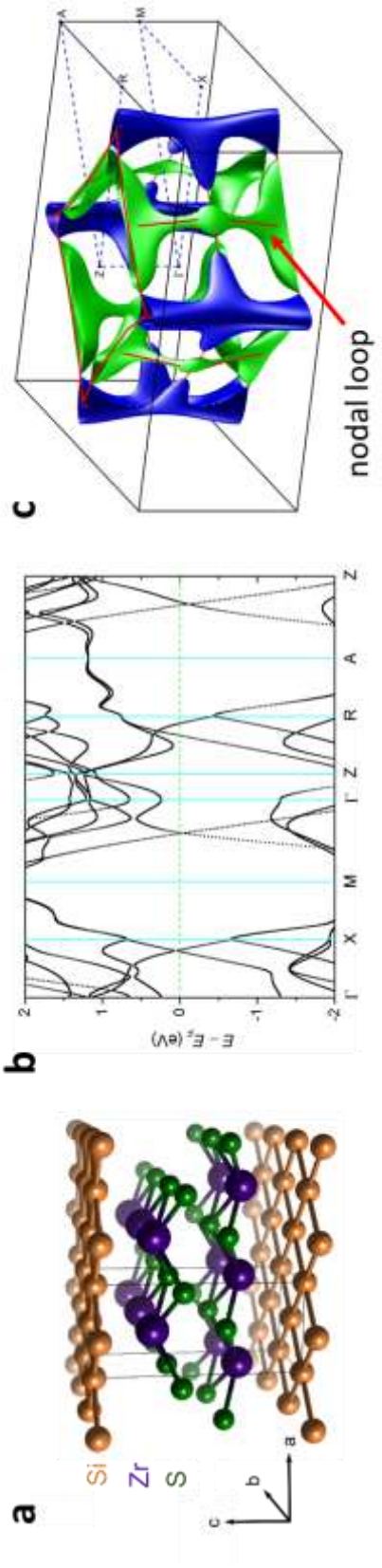

Figure 2

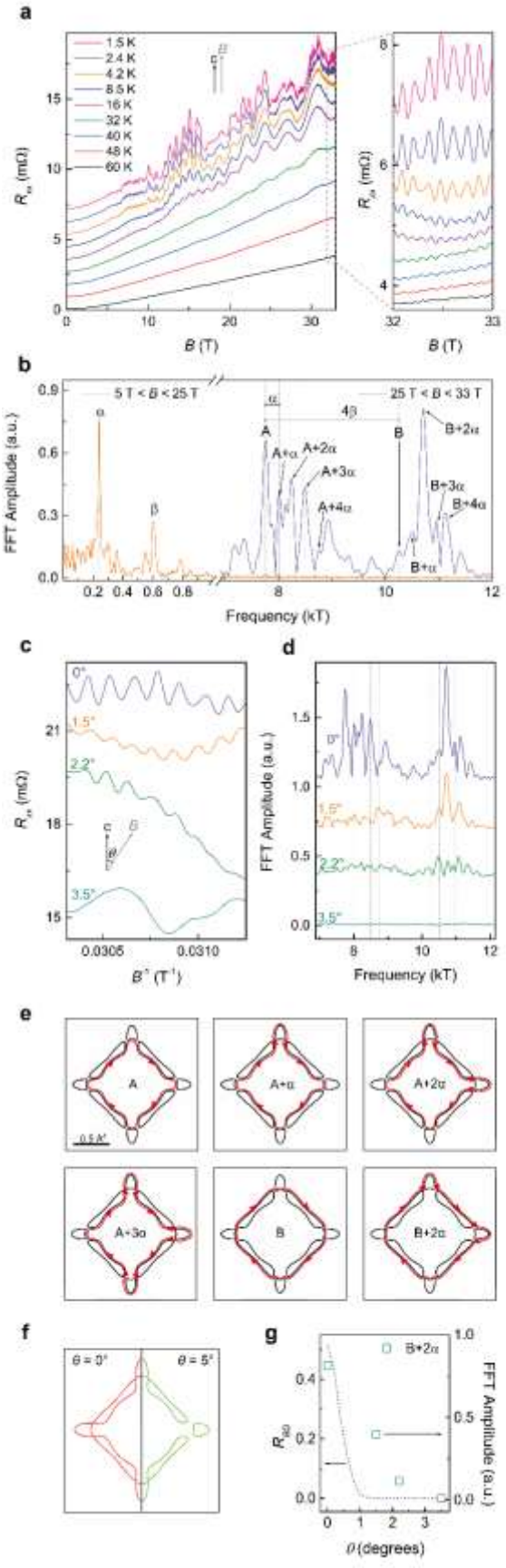
a
1.5 K
2.4 K
4.2 K
8.5 K
16 K
32 K
40 K
48 K
60 K
B
R_{xx} (mΩ)
B (T)
b
5 T < B < 25 T
25 T < B < 33 T
α
β
4β
A
A+α
A+2α
A+3α
A+4α
B
B+α
B+2α
B+3α
B+4α
FFT Amplitude (a.u.)
Frequency (kT)
c
0°
1.5°
2.2°
3.5°
B
B^{-1} (T^{-1})
d
FFT Amplitude (a.u.)
Frequency (kT)
e
A
A+α
A+2α
A+3α
B
B+2α
0.5 Å^{-1}
f
θ = 0°
θ = 5°
g
B+2α
$R_{2\theta}$
FFT Amplitude (a.u.)
θ (degrees)

Figure 3

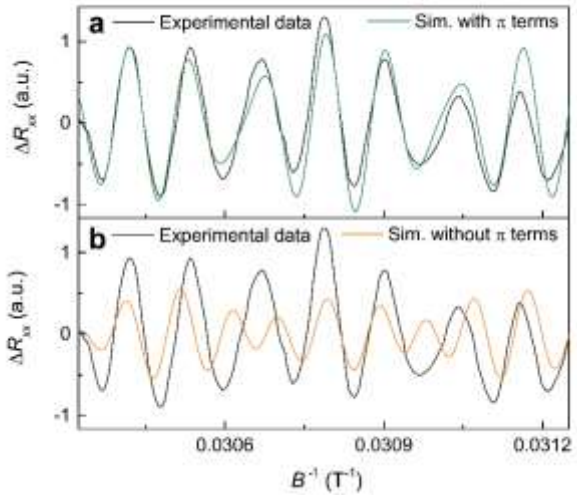

Figure 4

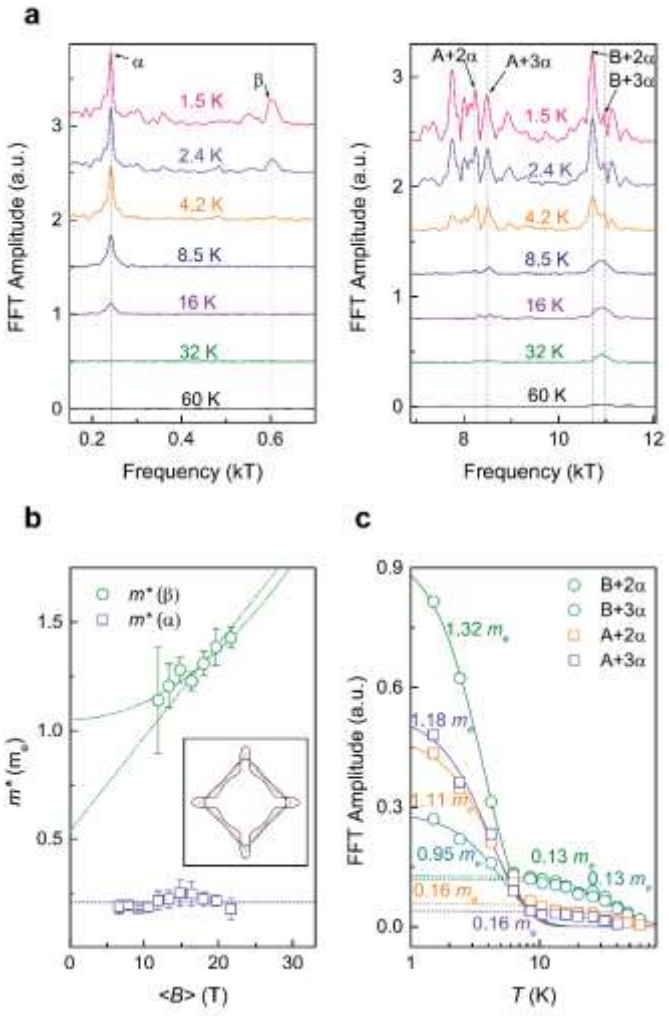

Figure Captions

Figure 1: **Crystallographic and electronic structure of ZrSiS**. (a) Crystal structure of ZrSiS. The Si square net is highlighted in light brown. (b) Calculated bulk band structure of ZrSiS with spin-orbit coupling. (c) Resultant three-dimensional Fermi surface. The top surface of the Brillouin zone contains the symmetry points Z, R and A. The location of the Dirac nodal loop is shown by the continuous red line.

Figure 2: **Shubnikov-de Haas oscillations and breakdown orbits in ZrSiS in a perpendicular magnetic field**. (a) Left panel: Series of magnetoresistance (MR) sweeps up to 33 T with **B**//*c* at the temperatures listed (curves are offset for clarity). Right panel: Close-up of the high-field part of the sweep, highlighting the fast oscillations that are associated with the onset of magnetic breakdown. (b) Fast Fourier transform (FFT) of the full MR sweep, having subtracted off a smooth polynomial background fit. The spectrum is divided into a low frequency part encompassing the frequencies due to the α (petal) pocket (F = 240 T) and β (dog-bone) pocket (F = 600 T) and a high frequency part that includes the frequencies of the breakdown orbits. The magnetic field ranges used for the two spectra are indicated in the figure. Label *A* corresponds to the "inner" breakdown orbits, *B* to the "outer" orbits as illustrated in Fig. 2(e). (c) Polar angle dependence of the high-field MR sweeps as a function of 1/B and (d) corresponding FFT spectra, showing the strong suppression of the high frequency (breakdown) oscillations with tilt angle. (e) Projection of the diamond Fermi surface at θ = 0° within the Z-R-A plane; the outer square represents the first Brillouin zone. Several of the breakdown orbits are indicated, their labels refer to the corresponding peaks in the FFT spectrum. (f) In-plane projection of the diamond Fermi surface for θ = 0° (left panel) and θ = 5° (right panel). In a tilted field, certain breakdown gaps increase in magnitude. (g) Attenuation of the oscillation amplitude as a function of θ. The solid line is a calculation of the damping term. See the Supplementary Information for more details.

Figure 3: **Geometrical (Berry) phase around a Dirac cone**. (a), (b) Black line: Oscillatory part of the magnetoresistance trace at 1.5 K (**B**//c), as a function of 1/B, between 32 T and 33 T. The green curve in (a) corresponds to $\sum_n a_n \cos(2\pi F_{A,n}/B + n\pi) + b_n \cos(2\pi F_{B,n}/B + n\pi)$, i.e. a sum of cosine functions with amplitudes (a_n and b_n) and frequencies ($F_{A,n}$ and $F_{B,n}$) given by the main peaks of the FFT in the right part of Figure 2b, and including a non-trivial Berry phase term ($n\pi$) for the breakdown orbits encircling an odd number of band-touching vertices. The

orange trace in (b) is obtained using the same function as the green one in (a), without the $n\pi$ terms. The two simulations include the orbits A, $A+\alpha$, $A+2\alpha$, $A+3\alpha$, $B+2\alpha$; the only free parameter is an initial phase factor, which is assumed to be equal for all cosine components.

Figure 4: **Effective mass and anomalous thermal damping of the oscillation amplitude**. (a) Fast Fourier transforms of the full magnetoresistance sweeps performed with **B**//*c* at the different temperatures listed for both the (left panel) low-frequency and (right panel) high-frequency oscillations (same magnetic field ranges of Fig. 2b). (b) Effective masses for the α and β pockets obtained from *T*-dependence of the oscillation amplitudes over different (inverse) field ranges whose mean is given by $\langle B \rangle = 1/[(1/B_{max} + 1/B_{min})/2]$. The ranges themselves, along with the fits to the LK expression, are presented in Fig. S9 of the Supplementary Information. The dashed and dotted lines are guides to the eye, under the assumption that the zero-field mass is unrenormalized or renormalized respectively. Inset: location of the nodal line (red line) within the in-plane projection of the diamond Fermi surface for **B**//*c*. (c) Mass plots for a number of frequencies corresponding to breakdown orbits. The solid and dashed lines are fits to the LK expression below and above T_0 = 8 K respectively. The quasiparticle masses extracted from each fit are given in the Figure.